Engineered Science

COMMUNICATION View Article Online

Zinc Stannate Nanorod as an Electron Transporting Layer for Highly Efficient and Hysteresis-less Perovskite Solar Cells

Mohammad Mahdi Tavakoli, *[1,2] Daniel Prochowicz, [3] Pankaj Yadav, [4] Rouhollah Tavakoli[1] and Michael Saliba [5]

Careful engineering of the electron transfer layer (ETL) is a promising approach to improve the efficiency of perovskite solar cells (PSCs). In this study, we demonstrate the potential of using zinc stannate (Zn_2SnO_4, or ZSO from here) as ETL for the fabrication of highly efficient PSCs. ZSO was deposited on top of FTO glass as thin films and nanorod arrays using ultrasonic spray pyrolysis (USP) technique. Optical characterizations reveal that perovskite films deposited on such nanorod arrays of ZSO have a lower transmittance exhibiting better charge extraction properties compared to the planar ZSO thin films. The best ZSO-based device reached a power conversion efficiency (PCE) of 18.24% and a high current density of 23.8 mA/cm^2. Moreover, these devices showed a lower hysteresis index in compared to the ZSO planar based devices.

Keywords: Perovskite; Solar cell; Efficiency; Zn_2SnO_4; Nanorod

Received 14th July 2018, Accepted 6th August 2018

DOI: 10.30919/es8d749

Reaching high efficiency and high stability are among the most important challenges in the field of organic-inorganic perovskite solar cells (PSCs).[1–5] The steady improvement is mainly reached using interface engineering, compositional engineering, crystal engineering and the utilization of passivation agents.[6–10] This recently results in a PSC device with a certified PCE of 22.6%.[11] Among these techniques, the improvement of charge extraction properties in electron transporting layer (ETL) and light absorption in the device are the most effective approaches for boosting the photovoltaic parameters of PSCs.[12–17] In general, TiO_2, ZnO, and SnO_2 are commonly used as ETLs for the fabrication of PSCs.[18–23] For example, Mahmood et al.[24] demonstrated a PSC using N-doped ZnO nanorods. This resulted in a PCE of 16.1% and low hysteresis. Jiang et al.[25] reported a PSC with an efficiency of 11.7% based on a TiO_2 nanowire ETL. Besides these metal oxides, Zn_2SO_4 (ZSO) is another alternative ETL for the fabrication of efficient PSCs, which has been recently utilized in the form of thin films and quantum dots (QDs). ZSO shows interesting electrical properties and its band levels are well-matched with perovskite absorber.[26–32] Bera et al.[31] deposited a compact layer of ZSO and reported a PCE of 13.34%, while Shin et al.[32] synthesized ZSO QDs at low temperature process resulting in a PCE of 15.3%.

[1] *Department of Materials Science and Engineering, Sharif University of Technology, 14588 Tehran, Iran. E-mail: mtavakol@mit.edu*
[2] *Department of Electrical Engineering and Computer Science, Massachusetts Institute of Technology, Cambridge, MA, USA. E-mail: mtavakol@mit.edu*
[3] *Institute of Physical Chemistry, Polish Academy of Sciences, Kasprzaka 44/52, 01-224 Warsaw, Poland*
[4] *Department of Solar Energy, School of Technology, Pandit Deendayal Petroleum University, Gandhinagar-382 007, Gujarat, India*
[5] *Adolphe Merkle Institute, Chemins des Verdiers 4, CH-1700 Fribourg*

In this work, we have successfully grown ZSO layers as thin films and in the form of nanorod arrays using an ultrasonic spray pyrolysis (USP) technique. We then employed them as ETLs for the fabrication of PSCs. The fabricated ZSO nanorods has a strong quenching effect in compared to ZSO based thin film indicating improved charge extraction. Moreover, PSCs based on ZSO nanorod photoelectrode exhibit a maximum PCE of 18.24% in compared to planar device with PCE of 17.04%, (mainly due to a higher current density).

Deposition of ZSO thin film and nanorod array: FTO glass (NSG-10) was selected as substrates for PSC devices. First, the substrates were etched by using zinc powder and HCl solution (2 M). Then, the substrates were cleaned carefully by 20 min sonication in Triton X100 (1 vol% in deionized water), deionized water, acetone, and ethanol, respectively. Ultrasonic spray pyrolysis was employed to fabricate ZSO planar film and nanorod array. In this regard, $ZnCl_2$ and $SnCl_2\,2H_2O$ (molar ratio = 2:1) were dissolved in 25 mL isopropanol (IPA). The concentration of solution was fixed to 0.1 M for both planar film and nanorod array. After 1 h stirring, the solution was sprayed on substrates using ultrasonic system and flowing oxygen as a carrier gas. The diameter of nozzle was 5 cm with many small holes. The substrate temperatures for thin film and nanorod array were 420 °C and 380 °C, respectively. The distance between nozzle and substrate was optimized and fixed for both cases (4 cm). For nanorod growth, we have reduced the gas pressure and increase the growth time as compared to thin film growth. Notably, for nanorod growth a seed layer of ZSO solution was spin-coated on the substrate, followed by annealing at 420 °C.

Device fabrication: After USP deposition of ZSO on the FTO glass and plasma cleaning for 2 min, $MAPbI_3$ perovskite was deposited from a solution of PbI_2 (1.2 M, TCI) and methylammonium iodide (1.15 M, dyesol) in a mixed solvent of DMF:DMSO (4:1). The spin

coating process was performed at 1000 rpm for 10 s and 6000 rpm for 30 s. 200 μL of chlorobenzene was applied to film 10 seconds before end of spinning. Then, the film was annealed at 100 °C for 1 h. For HTL layer, a solution of spiro (52 mg/500μL CB) with 23 μL of 4-*tert*-butyl pyridine (TBP) and 12.34 μL of bis(trifluoromethyl-sulfonyl)imide lithium salt (Li-TFSI, Sigma-Aldrich) (520 mg/1 mL acetonitrile) was spin-coated at 4000 rpm for 20 s (with ramp rate of 2000/s). The device was completed finally by thermal evaporation of 100 nm-thick gold as a back contact.

The ideality factor was calculated from the following formula:[40]

$$\mathrm{Ln}\left(\mathrm{I}\right) = \mathrm{Ln}\left(\mathrm{I}_0\right) + \left(\mathrm{q}/\mathrm{nkT}\right)\mathrm{V}$$

where I, I_0, q, n, k, T, and V are current, saturation current, electron charge, ideality factor, Boltzmann constant, temperature, and voltage, respectively.

Film characterization: The ZSO and perovskite morphologies were studied by scanning electron microscopy (SEM, ZEISS Merlin). Varian Cary 5 and Fluorolog 322 (Horiba Jobin Ybon Ltd) were employed to measure UV-vis and Steady-state photo-luminescence (PL) spectra, respectively. X-ray diffraction (XRD) pattern was measured by Bruker D8 X-ray Diffractometer (USA) utilizing a Cu $K\alpha$ radiation.

Device measurement: For J-V measurement a 450 W xenon lamp (Oriel, USA) and a digital source meter (Keithley model 2400, USA) were employed. All devices were measured using a black aperture with 0.1 cm^2 area. During the measurement, the scan rate was 10 mVs^{-1}. The intensity of lamp was 1000 W/m^2 for device measurement. The device was scanned from 0 to 1.2 V and reverse with a step size of 0.005 V and a delay time of 200 ms at each point.

ZnO based thin films and nanorod arrays are very promising ETL for the fabrication of highly efficient solar cells such as QDs, dye synthesized and polymer solar cells.[33–36] For PSCs, ZnO layer has a potential to react with perovskite film during the annealing process, as was shown by many researchers.[37,38] Fig. 1 shows the top-view scanning electron microscopy (SEM) images of perovskite films annealed on top of ZnO and ZSO ETLs. After the annealing process, the perovskite film on ZnO turned partially into a yellowish color indicating the presence of PbI_2 areas within the film. On the other hand, perovskite film on ZSO ETL was stable and did not show a yellow color. Thus, ZSO layer can be a great alternative to address the undesirable reaction of ZnO with perovskite.

In this study, we used USP to deposit ZSO layer as thin film and nanorod arrays. For the synthesis of nanorod arrays of ZSO, the FTO substrate temperature and gas pressure of the precursors were controlled as described in the Experimental Section. The substrate temperature for the fabrication of planar and nanorod ZSO was set at 420 °C and 380 °C, respectively. To grow nanorod ZSO layers, a very thin seed layer of ZSO was spin-coated on the substrate and annealed at 420 °C. Next, we lowered the grow rate of ZSO by decreasing the gas pressure and temperature to 380 °C. Fig. 2 depicts the top view SEM images of a planar film and a nanorod array of ZSO. The thin film of ZSO has an average grain size of 120 ± 20 nm with great crystallinity and compactness (Fig. 2a). On the other hand, the nanorod array of ZSO is dense and uniform with an average nanorod diameter of 30 ± 10 nm, as shown in Fig. 2b. To achieve high quality thin films

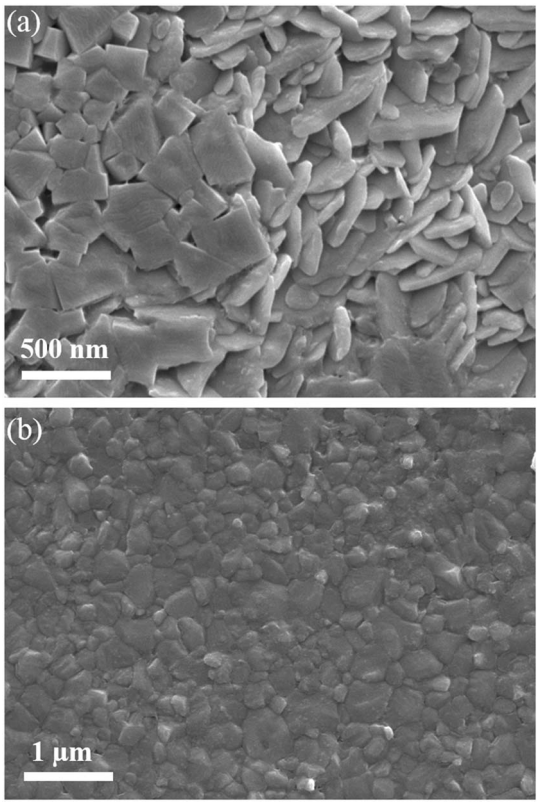

Fig. 1 Top-view SEM images of perovskite films deposited on (a) ZnO and (b) ZSO ETLs after annealing at 100 °C for 1 h.

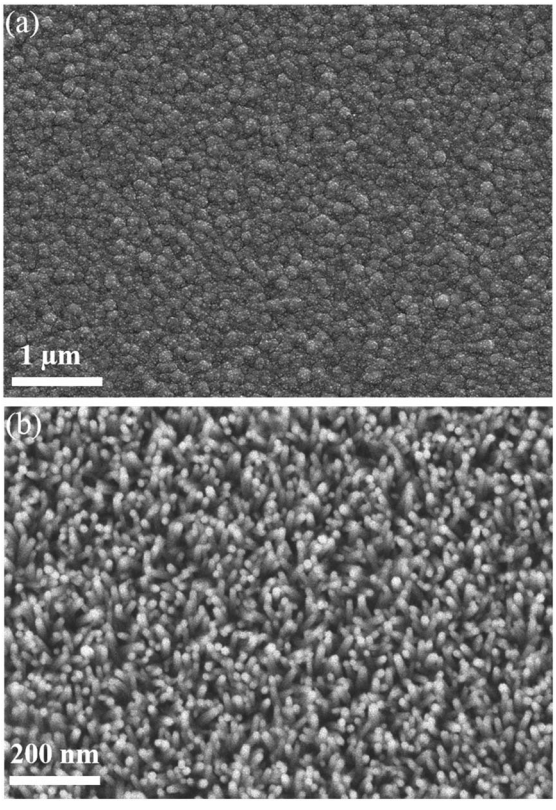

Fig. 2 Top-view SEM images of planar (a) and nanorod (b) ZSO ETLs deposited on glass using USP technique.

and nanorod ZSO ETLs, we have optimized various synthesis parameters. For instance, Fig. S1 shows the top-view SEM images of ZSO nanorod arrays obtained from a non-stoichiometric precursor solution at high concentration. To further study the quality of ZSO nanorod array, a powder x-ray diffraction (pXRD) pattern has been measured as shown in Fig. S2. Both ZSO planar and nanorod array show diffraction peaks located at 29.2°, 34.5°, 35.9°, 41.8°, and 55.2°, which are attributed to (220), (311), (222), (400) and (511) planes, respectively. These peaks are in good agreement with the reference peaks of ZSO film (ref code JCPDS-74-2184).[31] This result proves that ZSO layer has cubic spinel structure phase without any impurity of ZnO and SnO_2 phase. Notable, the broad background peak is from the glass substrate. Moreover, the ZSO nanorod array shows a strong peak in (311) direction, indicating the preferential orientation of nanorod array.

Fig. 3 shows the optical properties of the ZSO thin film and nanorod array. Interestingly, the transmittance of ZSO nanorod array in all wavelengths is higher than that obtained for the planar based ZSO (Fig. 3a). This indicates that the nanorod array helps to reduce the parasitic absorption of ZSO ETL and increase the absorption in a solar cell device. In the next step, a methylammonium lead triiodide ($MAPbI_3$) perovskite layer was deposited on top of the ZSO thin film and nanorod ETLs. Fig. S3 shows the absorbance spectrum of $MAPbI_3$ perovskite film with a band gap of 1.59 eV. The photoluminescence (PL) spectra of the perovskite films deposited on planar and nanorod ZSO ETLs are shown in Fig. 3b. We found that the nanorod array demonstrates a strong quenching effect as compared to planar ZSO samples. This suggests that the nanorod ETL can exhibit higher current density and lower hysteresis. To further confirm our PL result, we have performed time-resolved PL (TRPL) measurement for perovskite film deposited on planar and nanorod array ZSO. As shown in Fig. 3c, nanorod array shows stronger quenching effect as compared to planar sample, indicating its excellent charge transfer properties.

To study the effect of nanorod array on the photovoltaic properties, PSC devices based on planar and nanorod ZSO ETLs were fabricated. The device structure consists of FTO glass, ZSO ETL, $MAPbI_3$ absorber, spiro-OMeTAD hole transporting layer (HTL) and gold electrode. The current density-voltage (J-V) curves of the best performing PSC devices are shown in Fig. 4a. The champion planar device shows a short circuit current (J_{sc}) of 22.3 mA/cm^2, a V_{oc} of 1.06 V,

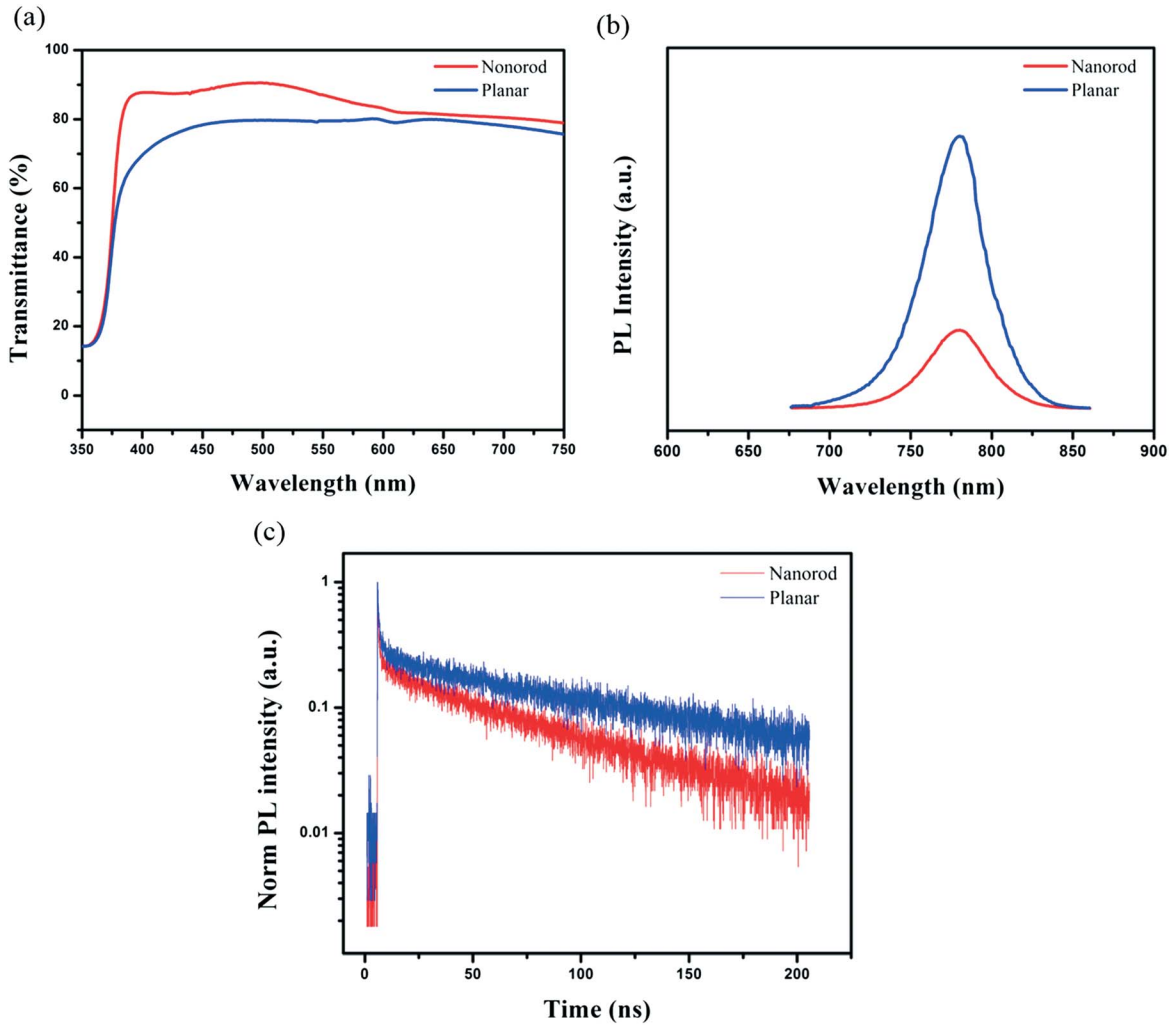

Fig. 3 (a) Transmittance spectra of planar and nanorod ZSO ETLs. (b) Photoluminescence spectra of perovskite films deposited on planar and nanorod ZSO ETLs. (c) Time-resolved PL spectra of the perovskite films on planar and nanorod ZSO ETLs.

a fill factor (*FF*) of 72.1% and a PCE of 17.04% (extracted from the reverse scan). Interestingly, the nanorod based device exhibits a high J_{sc} of 23.8 mA/cm^2, a V_{oc} of 1.05 V, a fill factor (*FF*) of 73% and a PCE of 18.24% (reverse scan). The figures of merit for the corresponding devices are also summarized in Table 1. These results demonstrate that the ZSO nanorod based device shows an enhanced J_{sc} and FF due to the higher absorption as well as better charge extraction properties. As we showed in Fig. 3a, the nanorod array has higher transmittance and thus higher absorption in nanorod device as compared to planar device. The observed slightly lower V_{oc} can be ascribed to the higher surface recombination. To confirm the high current density, we have performed an external quantum efficiency (EQE) test for the corresponding devices (Fig. 4b). Our results show that the calculated J_{sc} for planar and nanorod device are 21.7 and 23.1 mA/cm^2, respectively. These results are in good agreement with the values derived from the corresponding J–V measurement. In addition, we have calculated the

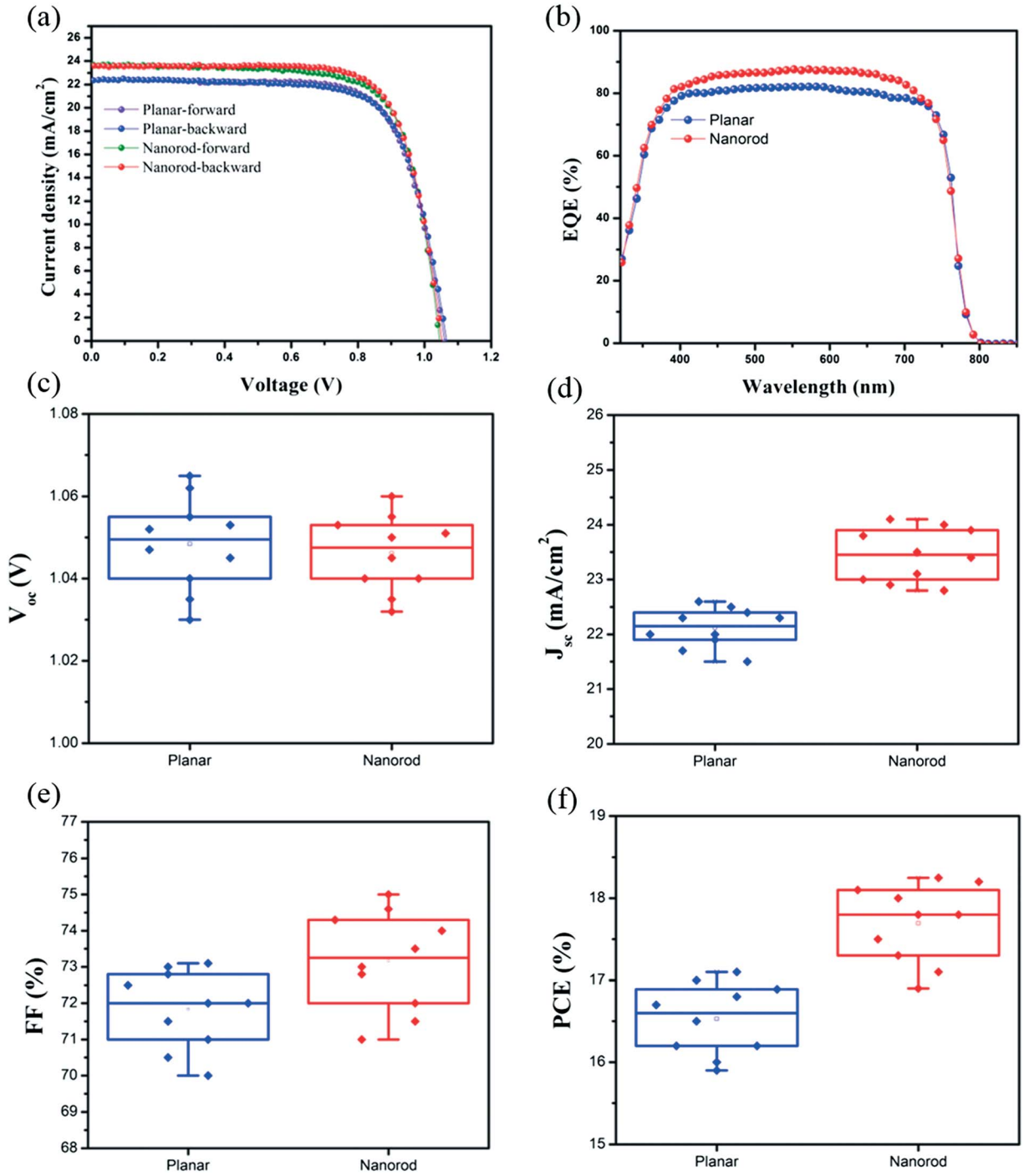

Fig. 4 (a) J-V curves and (b) external quantum efficiency spectra of PSC devices on planar and nanorod ZSO ETLs. (c-f) Distribution of photovoltaic parameters of PSC devices on planar and nanorod ETLs.

Table 1 Figure of merits for the best performing devices based on planar and nanorod Zn_2SnO_4 ETLs with forward and backward scan directions.

Sample	V_{oc} (V)	J_{sc} (mA/cm^2)	*FF* (%)	PCE (%)	Hysteresis index (%)
Planar-backward	1.06	22.3	72.1	17.04	2.28
Planar-forward	1.055	22.25	71	16.66	
Nanorod-backward	1.05	23.8	73	18.24	1.22
Nanorod-forward	1.047	23.7	72.6	18.02	

hysteresis index for the investigated devices as shown in Table 1 (hysteresis index = ($PCE_{backward}$-$PCE_{forward}$)/ $PCE_{forward}$)*100). We found that the ZSO nanorod based devices showed lower hysteresis as compared to ZSO planar based devices. In fact, ZSO nanorod array showed stronger quenching effect (see Fig. 3) and improved the charge extraction of electrons in the device as compared to planar ZSO. This may help to make a balance between electron and hole extraction in the device, resulting in lower hysteresis. Figs. 4c-4f show the distribution of photovoltaic parameters of PSC devices based on planar and nanorod array of ZSO ETL. The average values of photovoltaic parameters for 10 devices depict the same trend as the best performing devices, and the average values of J_{sc} (23.5 mA/cm^2), FF (73.2%), and PCE (17.8%) for ZSO nanorod based devices are higher than those of planar one. While the average value of V_{oc} for nanorod devices is slightly lower than planar ones. The reason of lower V_{oc} is the higher surface area on nanorod array as compared to planar device. More surface area can induce more defects (unbonded atoms), resulting in higher surface recombination.[39] Additionally, we have measured he dark current curves of the corresponding device and calculated their ideality factors (Fig. S4). The ideality factor for nanorod based device is less than (2.02) planar one (2.40). These results indicate that the nanorod based PSC shows slightly better diode behavior than planar device, resulting in better photovoltaic parameters.

One of the most important challenges in the PSC field which is necessary for commercialization is the device stability. In order to study the stability of nanorod based PSCs, we have performed shelf life stability test of nanorod based PSC devices after packaging with epoxy kept in dry box with 30% relative humidity over 60 days, as shown in Fig. 5. Our result shows that the nanorod device maintains 96% of it is initial PCE value after 2 months, indicating the potential of our device for commercialization.

In conclusion, we have employed USP technique for the fabrication of planar and nanorod ZSO ETLs and demonstrated their utilization for highly efficient PSCs. We found that ZSO ETL in the form of nanorod increases drastically the current density and FF of PSCs due to higher absorption and better charge transfer properties. The fabricated PSCs based on nanorod array of ZSO exhibited a maximum PCE of 18.24% with low hysteresis in compared to ZSO planar based device (17.04%). Our results demonstrate that ZSO layer in the form of planar thin film and nanorod array represents a great alternative ETL for the fabrication of efficient PSCs.

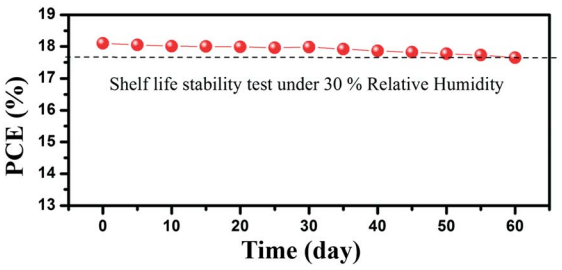

Fig. 5 Shelf life stability test of PSC device on ZSO nanorod array. After packaging by epoxy.

Conflicts of interest

There are no conflicts to declare.

Acknowledgement

M. M. T wants to thank Hong Kong University of Science and Technology and Sharif University of Technology for their supports. D. P. acknowledges support from the Marie Skłodowska Curie fellowship, H2020 Grant agreement no. 707168.

References

1 M. Saliba, T. Matsui, K. Domanski, J. Y. Seo, A. Ummadisingu, S. M. Zakeeruddin, J. P. Correa-Baena, W. R. Tress, A. Abate, A. Hagfeldt and M. Grätzel, *Science*, 2016, **354**, 206–209.
2 A. Waleed, M. M. Tavakoli, L. Gu, S. Hussain, D. Zhang, S. Poddar, Z. Wang, R. Zhang and Z. Fan, *Nano letters*, 2017, **17**, 4951–4957.
3 M. M. Tavakoli, S. M. Zakeeruddin, M. Grätzel and Z. Fan, *Adv. Mater.*, 2018, **30**, 1705998.
4 A. Waleed, M. M. Tavakoli, L. Gu, Z. Wang, D. Zhang, A. Manikandan, Q. Zhang, R. Zhang, Y. L. Chueh and Z. Fan, *Nano letters*, 2016, **17**, 523–530.
5 Q. Hou, J. Ren, H. Chen, P. Yang, Q. Shao, M. Zhao, X. Zhao, H. He, N. Wang, Q. Luo and Z. Guo, *ChemElectroChem.*, 2018, **5**, 726–731.
6 M. M. Tavakoli, A. Simchi, X. Mo and Z. Fan, *Mater. Chem. Front.*, 2017, **1**, 1520–1525.
7 Z. Wang, Q. Lin, F. P. Chmiel, N. Sakai, L. M. Herz and H. J. Snaith, *Nat. Energy*, 2017, **2**, 17135.
8 M. Yavari, M. Mazloum-Ardakani, S. Gholipour, M. M. Tavakoli, S. H. Turren-Cruz, N. Taghavinia, M. Grätzel, A. Hagfeldt and M. Saliba, *Adv. Energy Mater.*, 2018, **8**, 1800177.
9 N. J. Jeon, J. H. Noh, W. S. Yang, Y. C. Kim, S. Ryu, J. Seo and S. I. Seok, *Nature*, 2015, **517**, 476.
10 M. M. Tavakoli, D. Bi, L. Pan, A. Hagfeldt, S. M. Zakeeruddin and M. Grätzel, *Adv. Energy Mater.*, 2018, **8**, 1800275.
11 N. J. Jeon, H. Na, E. H. Jung, T. Y. Yang, Y. G. Lee, G. Kim, H. W. Shin, S. I. Seok, J. Lee and J. Seo, *Nat. Energy*, 2018, **3**, 682–689.
12 W. Hu, T. Liu, X. Yin, H. Liu, X. Zhao, S. Luo, Y. Guo, Z. Yao, J. Wang, N. Wang, H. Lin and Z. Guo, *J. Mater. Chem. A*, 2017, **5**, 1434.
13 M. M. Tavakoli, K. H. Tsui, Q. Zhang, J. He, Y. Yao, D. Li and Z. Fan, *ACS Nano*, 2015, **9**, 10287–10295.
14 M. Zhang, J. S. Yun, Q. Ma, J. Zheng, C. F. J. Lau, X. Deng, J. Kim, D. Kim, J. Seidel, M. A. Green and S. Huang, *ACS Energy Lett.*, 2017, **2**, 438–444.
15 M. M. Tavakoli, A. Simchi, Z. Fan and H. Aashuri, *Chem. Commun.*, 2016, **52**, 323–326.
16 J. Min, Z. G. Zhang, Y. Hou, C. O. Ramirez Quiroz, T. Przybilla, C. Bronnbauer, F. Guo, K. Forberich, H. Azimi, T. Ameri and E. Spiecker, *Chem. Mater.*, 2014, **27**, 227–234.
17 M. M. Tavakoli, R. Tavakoli, S. Hasanzadeh and M. H. Mirfasih, *J. Phys. Chem. C*, 2016, **120**, 19531–19536.
18 D. Prochowicz, P. Yadav, M. Saliba, D. J. Kubicki, M. M. Tavakoli, S. M. Zakeeruddin, J. Lewiński, L. Emsley and M. Grätzel, *Nano Energy*, 2018, **49**, 523–528.
19 M. M. Tavakoli, L. Gu, Y. Gao, C. Reckmeier, J. He, A. L. Rogach, Y. Yao and Z. Fan, *Sci. Rep.*, 2015, **5**, 14083.
20 P. Yadav, S. H. Turren Cruz, D. Prochowicz, M. M. Tavakoli, K. Pandey, S. M. Zakeeruddin, M. Grätzel, A. Hagfeldt and M. Saliba, *J. Phys. Chem. C*, 2018, **122**, 15149–15154.

21 M. M. Tavakoli, P. Yadav, R. Tavakoli and J. Kong, *Adv. Energy Mater.*, 2018, 1800794.

22 Y. Lee, S. Paek, K. T. Cho, E. Oveisi, P. Gao, S. Lee, J. S. Park, Y. Zhang, R. Humphry-Baker, A. M. Asiri and M. K. Nazeeruddin, *J. Mater. Chem. A*, 2017, **5**, 12729–12734.

23 M. M. Tavakoli, F. Giordano, S. M. Zakeeruddin and M. Grätzel, *Nano Lett.*, 2018, **18**, 2428–2434.

24 K. Mahmood, B. S. Swain and A. Amassian, *Adv. Energy Mater.*, 2015, **5**, 1500568.

25 Q. Jiang, X. Sheng, Y. Li, X. Feng and T. Xu, *Chem. Commun.*, 2014, **50**, 14720–14723.

26 S. S. Mali, C. S. Shim and C. K. Hong, *Sci. Rep.*, 2015, **5**, 11424.

27 L. Li, L. Gu, Z. Lou, Z. Fan and G. Shen, *ACS Nano*, 2017, **11**, 4067–4076.

28 L. S. Oh, D. H. Kim, J. A. Lee, S. S. Shin, J. W. Lee, I. J. Park, M. J. Ko, N. G. Park, S. G. Pyo, K. S. Hong and J. Y. Kim, *J. Phys. Chem. C*, 2014, **118**, 22991–22994.

29 V. V. Ganbavle, M. A. Patil, H. P. Deshmukh and K. Y. Rajpure, *J. Anal. Appl. Pyrolysis*, 2014, **107**, 233–241.

30 S. S. Shin, D. W. Kim, D. Hwang, J. H. Suk, L. S. Oh, B. S. Han, D. H. Kim, J. S. Kim, D. Kim, J. Y. Kim and K. S. Hong, *Chem. Sus. Chem.*, 2014, **7**, 501–509.

31 A. Bera, A. D. Sheikh, M. A. Haque, R. Bose, E. Alarousu, O. F. Mohammed and T. Wu, *ACS Appl. Mater. Interfaces*, 2015, **7**, 28404–28411.

32 S .S. Shin, W. S. Yang, J. H. Noh, J. H. Suk, N. J. Jeon, J. H. Park, J. S. Kim, W. M. Seong and S. I. Seok, *Nat. Commun.*, 2015, **6**, 7410.

33 M. M. Tavakoli, H. Aashuri, A. Simchi and Z. Fan, *Phys. Chem. Chem. Phys.*, 2015, **17**, 24412–24419.

34 M. M. Tavakoli, A. Simchi and H. Aashuri, *Mater. Chem. Phys.*, 2015, **156**, 163–169.

35 Y. J. Noh, S. I. Na and S. S. Kim, *Sol. Energy Mater. Sol. Cells*, 2013, **117**, 139–144.

36 M. M. Tavakoli, A. Simchi, X. Mo and Z. Fan, *Mater. Chem. Front.*, 2017, **1**, 1520–1525.

37 F. Yang, D. W. Kang and Y. S. Kim, *RSC Advances*, 2017, **7**, 19030–19038.

38 M. M. Tavakoli, R. Tavakoli, Z. Nourbakhsh, A. Waleed, U. S. Virk and Z. Fan, *Adv. Mater. Interfaces*, 2016, **3**, 1500790.

39 M. M. Tavakoli, Q. Lin, S. F. Leung, G. C. Lui, H. Lu, L. Li, B. Xiang and Z. Fan, *Nanoscale*, 2016, **8**, 4276–4283.

40 O. Almora, K. T. Cho, S. Aghazada, I. Zimmermann, G. J. Matt, C. J. Brabec, M. K. Nazeeruddin and G. Garcia-Belmonte, *Nano Energy*, 2018, **48**, 63–72.